Plasmonic Color Filter and its Fabrication for Large-Area Applications

Yun Seon Do, Jung Ho Park, Bo Yeon Hwang, Sung-Min Lee, Byeong-Kwon Ju, and Kyung Cheol Choi**

With the great interest in "plasmonics", metallic nano structures have been used for optical applications. The accompanying optical resonance, known as surface plasmon resonance (SPR), has highly motivated researchers because this unique optical phenomenon shows strong interaction with lights within a tiny volume of space. Surface plasmons (SPs) in optically thin metal films contribute to extraordinary optical transmission (EOT) through subwavelength apertures.[1] Therefore, researchers have suggested plasmonic color filters (PCFs) with a selective filtering function in subwavelength metallic holes.[2–6]

Color filters, widely used for the industrial devices such as organic light emitting diodes, liquid crystal displays, and CMOS image sensors, are composed of organic dyes. The filtering performance originating from the color sensitivity of the dyes is degraded by heat and ultraviolet radiation due to the low chemical stability of the organic materials.[7] In addition, the complex structure requires a highly-accurate aligned lithography to spatially separate colors by pixel unit.

On the other hand, PCFs have an optically thin metal layer, and their transmittance can be tuned by the geometrical and material conditions: the periodicity, size and shape of holes, the thickness of metal, and the optical constants of the materials. This simple and thin structure is advantageous for assembly into other devices without worry about degradation by heat and light. More recently, PCFs integrated on top of the CMOS image sensor have been reported,[6] and experimental analysis of spatial cross talk and the effect of defect has been performed in detail.[5] These results have shown greater possibility for PCFs in industrial applications. However, the fabrication methods used up to now to make plasmonic structures, such as nanoimprinting,[8] electron beam lithography[2–6] or the focused ion beam method,[1,9] restrict mass-production of PCFs, leading to problems of low speed, small patterning area, and high cost of equipment.

Y. S. Do,[+] S.-M. Lee, Prof. K. C. Choi
Department of Electrical Engineering
KAIST, Daejeon, 305–701, Republic of Korea
E-mail: kyungcc@kaist.ac.kr
J. H. Park,[+] B. Y. Hwang, Prof. B.-K. Ju
School of Electrical Engineering
Korea University,
Seoul, 136–713, Republic of Korea
E-mail: bkju@korea.ac.kr
[+] These authors contributed equally to this work.

DOI: 10.1002/adom.201200021

Here we suggest a fabrication flow including a laser interference lithography (LIL) step. Contrary to above-mentioned technologies, LIL, with simple maskless equipment, yields perfect ordering patterns, which are, as they must be, spatially coherent over a large area. Although LIL has a limitation in that it can only fabricate simple periodic patterns, it is an attractive additional solution to add to the conventional methods for applications in which periodic patterns are desirable.[10] In this regard, fabrication of plasmonic color filters with LIL enables us to suggest the easiest method to achieve large size PCFs without losing performance aspect. Additionally, a single pixel of the PCFs can be reduced to 1 μm-size;[5] the interference pattern, with a period of hundreds of nm, is small enough to separate the patterned area into pixel units. Thus, it is possible to effect spatial separation of colors by simple shadow masking and multi exposure. More complicated microscale patterns with nano-holes can be fabricated by soft interference lithography.[11]

Albeit many reported results show an easy tunability of transmittance, they provide fewer explanations to help in the optimization of EOT in PCFs with metallic holes, which are experimentally realizable. In this work, we offer a structure in which SP modes at the metal-dielectric interfaces occur simultaneously, allowing for efficient EOT and resulting in optimized filtering characteristics. We use the dielectric material which is different from the material of substrate. The designed PCFs, with primary colors, are demonstrated on an area of 2.5 cm × 2.5 cm.

The spectral response of a square array includes multiple transmittance peaks with central wavelength, λ_{max}, approximated by[12]

$$\lambda_{\max(i,j)} = \frac{P}{\sqrt{i^2 + j^2}} \sqrt{\frac{\varepsilon_m \varepsilon_d}{\varepsilon_m + \varepsilon_d}} \quad (1)$$

where P is the period of the array, and ε_m and ε_d are the permittivity of metal and dielectric layer respectively; the (i, j) number originated from the reciprocal vectors in the 2D array determines the resonance modes. The longest λ_{max} ($\lambda_{max(1,0)}$ or $\lambda_{max(0,1)}$) was used as the pass band of the filter. Because Equation 1 is missing the presence of the holes and the associated scattering losses, the calculated λ_{max} is different from that of the experimental results.[13] However, we can refer to this calculated value to predict the relative position between the transmittance peaks. We used aluminium (Al) with a high plasma frequency and lithium fluoride (LiF) with a smaller permittivity than that of the glass substrate in order to achieve shorter λ_{max}.

There are two different sets of transmittance peaks in the PCF: λ_u, due to the SP mode bounded to the upper metal-dielectric interface (SP_u), and λ_b from the SP modes at

COMMUNICATION

the interface of the bottom (SP_b). The transmittance of the pass band can be enhanced by the same dielectric boundaries, i.e., λ_u and λ_b are the same.[14] The enhancement of the transmittance was achieved by deposition of the same dielectric material[3] or by using matching oil.[2] Another group used a perforated dielectric layer on top of the metal film for the matching layer, as well as a mask to etch hole patterns in the metal film.[4] Despite these experimental attempts, more detailed analysis of the SP modes is required to design an optimized transmittance.

We performed numerical simulation of the aforementioned two approaches in order to determine the most efficient structure for matching SP modes. All structures were consisted of a 50 nm thick LiF layer and a 150 nm thick Al layer on a glass substrate. The period of the hole arrays was 390 nm and the diameter of the holes was 220 nm. The thickness of the LiF layer on the upper interface was varied from 10 nm to 200 nm. **Figure 1** illustrates the spectral responses and profile images of the electric field intensity of each structure, as indicated in insets of Figure 1a,d,g. Since the sample holder was rotated during the evaporation of the LiF for the structure shown in Figure 1g, we assumed that the same thickness of LiF was deposited on the cylindrical wall in the hole as well as on the top surface of the metal. We made one more assumption that the top of the PCF became planar when the thickness of the deposited LiF was larger than the thickness of the Al layer, 150 nm.

When the metal film was exposed to the air, the electric field highly concentrated around the bottom of the hole due to the $SP_{b(1,0)}$ at the longest wavelength, λ_1 (606 nm). At the second

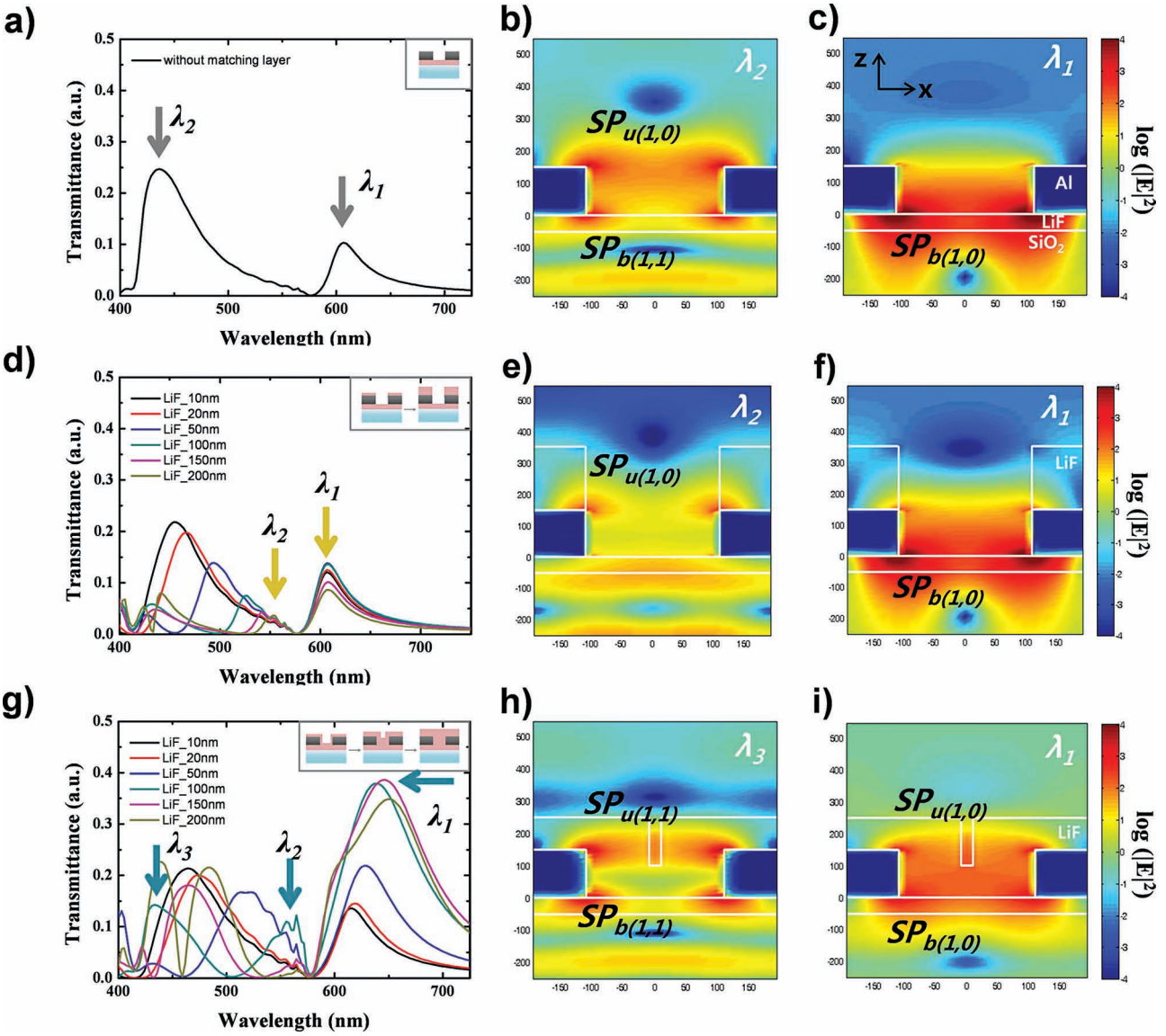

Figure 1. Calculated transmittance and electric field intensity on x-z planes (at the center of the holes) with various conditions of the upper dielectric layer: (a), (b), and (c) are for the PCFs without the upper LiF layer; (d), (e), and (f) are for the PCFs with the upper LiF layer that has hole patterns the same as those of the metal layer; (g), (h) and (i) are for the PCFs of which the cylindrical surface as well as the top surface are covered with LiF.

longest wavelength, λ_2 (435 nm), strong field distribution occurred at both the top and bottom of the hole, as shown in Figure 1b. The smaller permittivity of air resulted in the SP_u at a shorter wavelength than that of the SP_b at the glass-Al interface, and that gave rise to the $SP_{u(1,0)}$ at around λ_2. In addition, considering Equation (1) and λ_1, λ_2 corresponds well to the $SP_{b(1,1)}$. The transmittance was enhanced more efficiently at λ_2, where the $SP_{b(1,1)}$ and $SP_{u(1,0)}$ occurred at the same time.

Figure 1d shows the transmittance of the structure, of which the upper LiF layer consisted of the same hole patterns as those of the Al layer. As the thickness of the LiF increased, the peak position of λ_2 showed a red-shift, and the transmittance rapidly decreased while the transmittance of λ_1 decreased without a shift. The thickness of the upper LiF was scaled on the order of the penetration depth of SP, δ_d.[15] Thus, the upper LiF layer affected the effective permittivity, ranging from that of air to that of LiF. That resulted in a red-shift of the λ_2 with a thicker LiF layer. However, the SP_b and SP_u were still separated at λ_1 and λ_2, respectively, even with a 200 nm thick layer of LiF, as shown in Figure 1e–f.

On the other hand, large enhancement of the transmittance at λ_1 was detected when holes were filled and surrounded with LiF (Figure 1g). As the LiF got thicker, the peak at λ_1 slightly shifted to the longer wavelength. In addition, the noticeable $SP_{u(1,0)}$ as well as the $SP_{b(1,0)}$ concurrently appeared at λ_1 when the LiF was thicker than 50 nm, whilst the transmittance increased. A similar amount of field distribution was shown in the top and bottom of the hole with the 100 nm thick layer of LiF (Figure 1i), and that maximized the transmittance at λ_1. The $SP_{b(1,1)}$ and $SP_{u(1,1)}$ also occurred simultaneously at λ_3 (Figure 1h). The matched SP_b and SP_u were maintained after planarization (Supporting Information Figure S1e-h). As a greater amount of LiF surrounded the hole, the SP_u became weaker with accompanying the red-shifted λ_2 (Supporting Information Figure S1c). In our simulation, $\delta_{d(LiF)}$ was varied from 228 nm to 415 nm in the 400–700 nm wavelength range. We believe that the dielectric media has to be continuous from the metal-dielectric interface on the order of the δ_d for the sake of matching SP_b and SP_u modes. After maximization, the transmittance at λ_1 decreased. For the experiment, we deposited LiF up to 150 nm to allow for planarization with maximum transmittance.

The thickness of the LiF at the bottom metal-dielectric interface had a relatively small effect on the SP_b (Supporting Information Figure S2). We deposited a 50 nm thick layer of LiF on the glass substrate in order to reduce the roughness at the surface for the experimental.

Figure 2 shows the suggested fabrication procedure. A LiF layer (50 nm) and an Al layer (150 nm for the red and green; and 100 nm for the blue) were thermally evaporated in sequence on the glass substrate. In the following, laser inference lithography was performed with a Lloyd's mirror interferometer system.[16] To make the interference patterns, two beams were used: one travels directly to the specimen and the other was reflected onto the specimen by the mirror. These two beams formed a 1D interference pattern on the specimen.[17] The periodicity, P, of the pattern is determined by,[18]

$$P = \frac{\lambda}{2 \cdot \sin\theta} \tag{2}$$

where λ is wavelength of the laser and θ is the incident angle of the mirror to the specimen. A single exposure generated a 1D line pattern and 2D dot/hole patterns were generated from successive exposures with 90° rotation of the sample. After development, circular holes were patterned. For matching SP modes, LiF was deposited to a thickness of 150 nm by thermal evaporation after etching Al and removing photoresist.

From the viewpoint of determining the pass band, P is the main factor to determine the position of λ_{max}. In our experiment, the laser exposure was performed with four different values of θ: 20°, 25°, 30°, and 35°, and each condition corresponded to the length of P: 390 nm, 320 nm, 260 nm and 230 nm, respectively (Supporting Information Figure S3). For the given values of P, the spectral curves were tuned by adjusting the thickness of the metal layer and the size of the holes (Supporting Information 4). PCFs with metallic hole arrays showed a trade-off in transmittance and bandwidth. Additionally, the SPR structure accompanied additional transmittance peaks at the shorter wavelength, resulting in a degradation of the color purity for the red and green filters. We optimized the thickness of the Al layer and the size of holes using the following rules: 1) Maximum transmittance of the target color was at least 1.5 times larger than that of the undesirable peaks; 2) full-width at

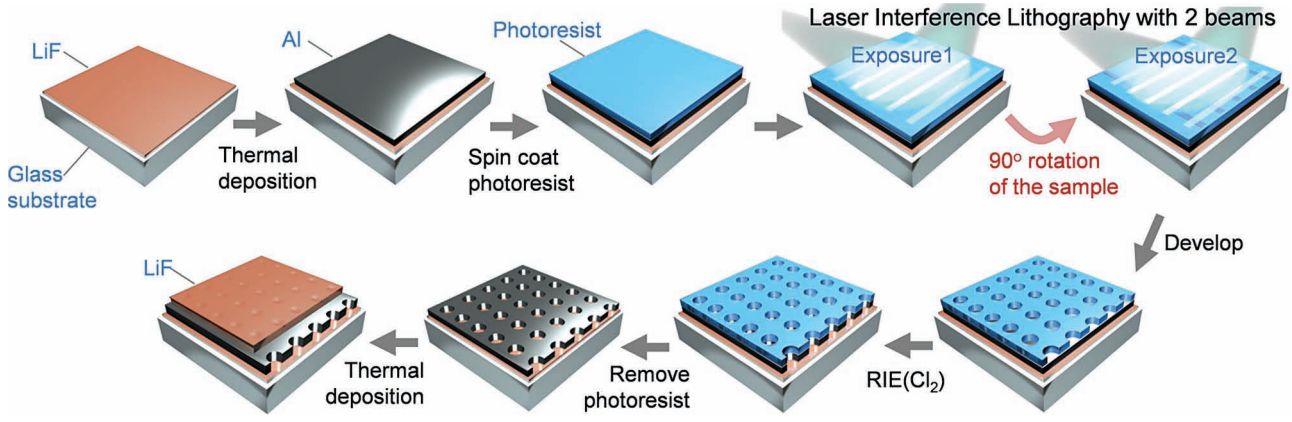

Figure 2. Schematic diagram of the proposed fabrication process. In a Lloyd's mirror interferometer system, two laser beams form an 1D interference pattern on the specimen. To create array patterns with a square symmetry, two exposures by a rotation of 90° in between are applied.

Table 1. The dimensions of the optimized structure for each color. The average values of the diameter of the holes in the fabricated samples were rounded off to the tens place.

	Period (P) [nm]	Thickness of Al [nm]	Diameter of holes [nm]	Diameter of holes (Experimental) [nm]
Red	390	150	200~230	~210
Green	320	150	180~200	~180
Blue	230	100	120~160	~120

half-maximum (FWHM) came under the wavelength range of: smaller than 500 nm for the blue, 500 nm to 600 nm for the green, and larger than 600 nm for the red.

The optimized dimensions for each structure are specified in **Table 1**. The last column indicates the average hole size, which was patterned on the photoresist. The size of the hole can be tuned by adjusting the exposure dosage, the beam power and the time for developing.

As shown in **Figure 3**b, we obtained 21.6%, 19.9%, and 22.9% for the maximum transmittances of the red, green, and blue, respectively. The center wavelengths of the pass bands correspond well to the simulation results shown in Figure 3a. However, the maximum transmittance dropped to 0.65 (red), 0.56 (green), and 0.73 (blue) times as high as the simulated value, and the bandwidth of the red and blue filters broadened.

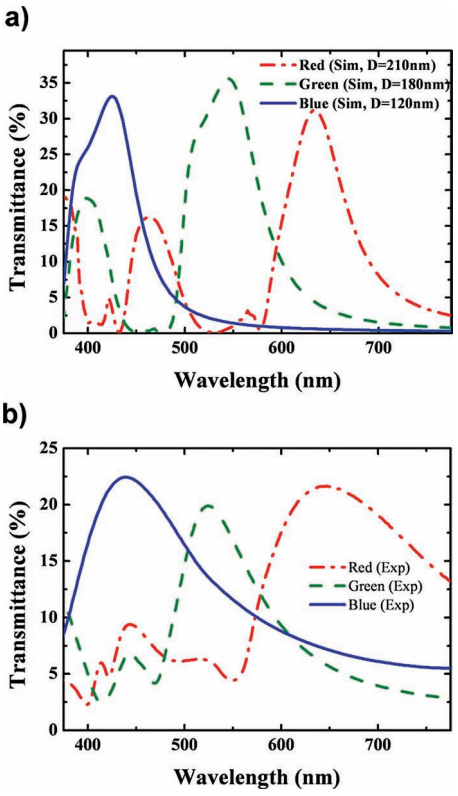

Figure 3. Transmittance spectra of (a) the simulated and (b) the fabricated PCFs. For the experimental results, the average values of the diameter of holes were 210 nm, 180 nm, and 120 nm for the red, green, and blue filters, respectively.

For the red filter, the harmonics of the SPR obstruct the filtering of red color only, rather than large FWHM (over 200 nm). FWHM of the green filter was 100 nm. The thinner metal of the blue filter was accompanied by a large FWHM (150 nm) and by a long tail of the pass band.

The differences between calculations and experimental results are due to the imperfection of the fabrication: roughness of all deposited layers, the shapes of holes, and uniformity of the shape and size of holes. Unlike our assumption, the top of the fabricated sample was wavy, as shown in **Figure 4**a. We checked the effect of the surface morphology by a FDTD simulation

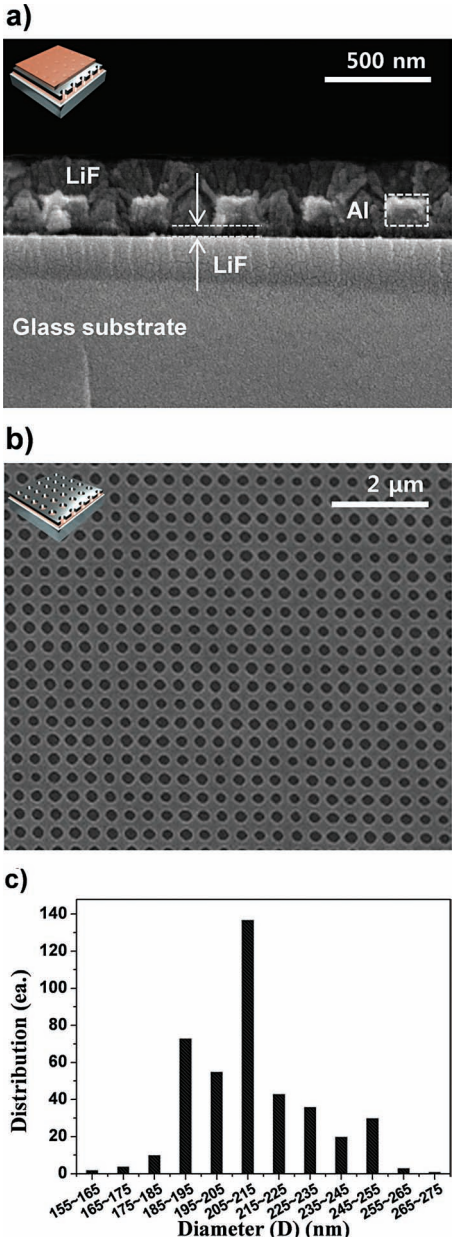

Figure 4. Scanning electron microscope (SEM) images of the red PCF: (a) cross-section after completing the fabrication process, (b) surface of the Al layer after RIE and removal of the photoresist, (c) A distribution diagram of the size of the holes in (b).

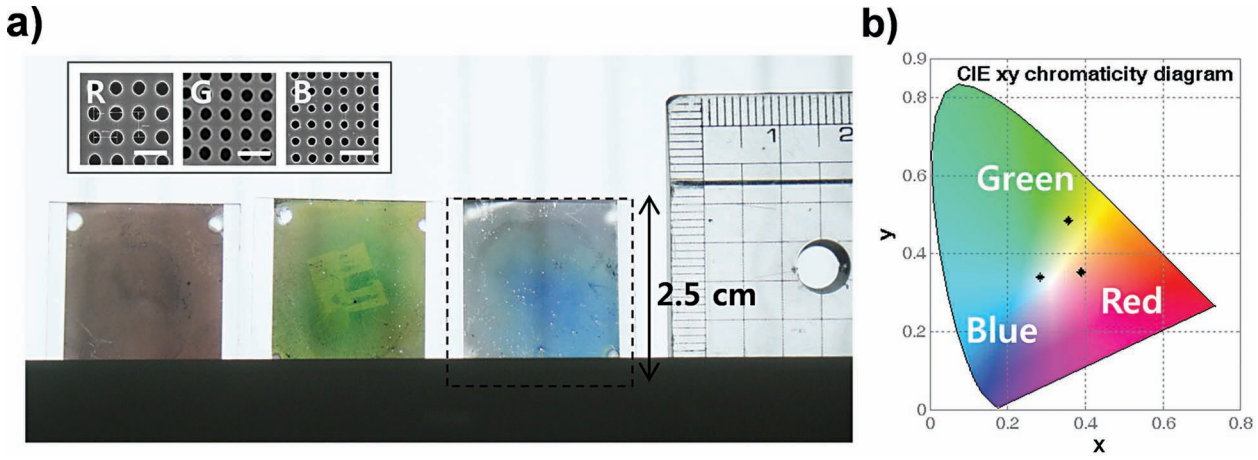

Figure 5. Chromaticity characteristics of the PCFs. (a) Photograph of PCFs: the red, green, and blue from the left. The vertical blind in the background shows through the filters. Dashed line represents the boundary of the sample. Insets are the scanning electron microscope (SEM) images of the photoresist of each filter, with a white scale bar of 500 nm. b) CIE chromaticity diagram of the fabricated PCFs. Each color corresponds to the point of (x, y): (0.3896, 0.3523) for the red, (0.3559, 0.4841) for the green, and (0.2836, 0.3384) for the blue.

(Supporting Information Figure S5). Although the amount of extracted light from the structure changed slightly according to the surface morphology, this result cannot sufficiently explain the distinctive decrease in the transmittance of the experimental results. On the other hand, as shown in Figure 4b and c, the pattern on the metal had relatively poor uniformity in hole size. Poor uniformity can be understood by considering the defects. Similar to the effects of random defects,[5] our experimental structure resulted in a quite small transmittance and broader bandwidth compared to that predicted by the simulation. LIL was performed in a normal laboratory environment without any equipment controlling for contamination and vibration. Since the interference pattern dealt with in our experiment is sized in the sub-microns, light scattering by such things as only a little dust, weak air vibration, or an earth tremor could cause an interruption of patterning uniformly over the whole area. The experimental environment for the exposure of light has to be improved in consideration of these issues in order to obtain better uniformity and reproducibility of the patterning.

Figure 5a provides the photograph of the PCFs. The color gamut of each filter was mapped on the CIE 1931 xy chromaticity diagram (Figure 5b). As with the transmittance results, the red and blue filters showed worse color purity compared to that of the green filter. Since Z, which is quasi-equal to the blue stimulation, is the biggest among the tristimulus values, the blue-noise light can have the worst effect on the color purity. In the hexagonal arrays, the transmittance peaks originating from the 1st and 2nd resonance modes are split into further position in wavelength region than are the square arrays.[12] This would be advantageous for producing pure red color. Fortunately, three laser beams make a 2D interference pattern with a hexagonal array, so there is chance, experimentally, to improve the color purity.

In conclusion, we demonstrate a large area plasmonic color filter highly adaptable to industrial applications. In order to achieve high efficiency of the EOT in the metallic holes, the dielectric material has to surround not only each metal-dielectric interface but also the cylindrical wall of the hole on the order of δ_d. This thin and quasi-plane structure would be advantageous when integrated onto other devices. The LIL process provides nano-scaled array patterns through the whole area of 2.5 cm × 2.5 cm. This is extremely large compared to the area of previous plasmonic devices, and there is the possibility of enlarging the patterning area.[19] Because the fabricated hole array shows high accuracy and good regularity of period, the pass band is thought to correspond well to that predicted in the calculations. Although the poor uniformity in the size of the holes results in low transmission and broad bandwidth, the results show high feasibility for PCFs to be applicable to the industrial devices. We expect that these results will provide the opportunity to bring together the proper nanotechnologies in mass production, and lead to advances in optical devices.

Experimental Section

A LiF layer (50 nm) and an Al layer (150 nm for the red and green; 100 nm for the blue) were thermally evaporated in sequence on the glass substrate. Adhesion layer was coated (HMDS:PGMEA = 1:4) before the photoresist (AR-N4240, mixed with Thinner AR 300–12 at a ratio of 1:1) was spin-coated onto the sample, yielding a resist thickness of 300 nm.

In what follows, the samples were exposed in a Lloyd's mirror interferometer. The laser used for exposure was a frequency-doubled argon-ion laser with a wavelength of 257 nm and an output power of 0.16 mW/cm^2. The desired power was set using an optical power/energy meter (Newport, 1936-C), and, with the sample loaded, the exposure was initiated. The light is directed through a spatial filter; the focusing distribution of the initial laser beam is approximately 0.15 mm, the focal length of the focusing length is 3.4 mm, and the distance between the spatial filter and the sample holder is around 1.2 m. For our setup, the typical exposure time is 140 s. Because two beams form a 1D interference pattern on the specimen, 2D hole patterns were generated from successive exposures with 90° rotation of the sample. After development, circular holes with diameter of 210 nm were patterned every 390 nm when θ was equal to 20°.

Next, chlorine (Cl_2) based inductive coupling plasma reactive ion etching (ICP-RIE, TCP-9600DFM, Lam Research) was performed to etch the Al. The photoresist, which was plasma-treated during RIE, was removed by air plasma (PDC-32G-2, Harrick Plasma). Finally, LiF was deposited to a thickness of 150 nm by thermal evaporation.

The transmittance spectra of the fabricated filters were measured with a spectrophotometer (UV-2550, Shimadzu). The color gamut of each filter was checked using a luminance colorimeter (BM7-A, TOPCON).

Supporting Information

Supporting Information is available from the Wiley Online Library or from the author.

Acknowledgements

This research was supported by Basic Science Research Program through the National Research Foundation of Korea (NRF) funded by the Ministry of Education, Science and Technology (CAFDC-20120000820). Additionally, this work was supported by the IT R&D program of MKE/KEIT (Grant No. 10041416) and the Industrial Strategic Technology Development Program (KI002104).

Received: October 24, 2012
Revised: November 15, 2012
Published online: February 12, 2013

[1] T. W. Ebbesen, H. J. Lezec, H. F. Ghaemi, T. Thio, P. A. Wolff, *Nature* **1998**, *391*, 667.
[2] H. S. Lee, Y. T. Yoon, S. S. Lee, S. H. Kim, K. D. Lee, *Opt. Express* **2007**, *15*, 15457.
[3] Q. Chen, D. R. S. Cumming, *Opt. Express* **2010**, *18*, 14056.
[4] D. Inoue, A. Miura, T. Nomura, H. Fujikawa, K. Sato, N. Ikeda, D. Tsuya, Y. Sugimoto, Y. Koide, *Appl. Phys. Lett.* **2011**, 98.
[5] S. Yokogawa, S. P. Burgos, H. A. Atwater, *Nano Lett.* **2012**, *12*, 4349.
[6] a) Q. Chen, D. Chitnis, K. Walls, T. D. Drysdale, S. Collins, D. R. S. Cumming, *IEEE Phot. Technol. Lett.* **2012**, *24*, 197; b) Q. Chen, D. Das, D. Chitnis, K. Walls, T. D. Drysdale, S. Collins, D. R. S. Cumming, *Plasmonics* **2012**, *7*, 695.
[7] R. W. Sabnis, *Displays* **1999**, *20*, 119.
[8] H. J. Park, T. Xu, J. Y. Lee, A. Ledbetter, L. J. Guo, *ACS Nano* **2011**, *5*, 7055.
[9] T. Xu, Y. K. Wu, X. G. Luo, L. J. Guo, *Nat. Commun.* **2010**, 1.
[10] a) M. L. Schattenburg, C. R. Canizares, D. Dewey, K. A. Flanagan, M. A. Hamnett, A. M. Levine, K. S. K. Lum, R. Manikkalingam, T. H. Markert, H. I. Smith, *Opt. Eng.* **1991**, *30*, 1590; b) M. Campbell, D. N. Sharp, M. T. Harrison, R. G. Denning, A. J. Turberfield, *Nature* **2000**, *404*, 53; c) I. B. Divliansky, A. Shishido, I. C. Khoo, T. S. Mayer, D. Pena, S. Nishimura, C. D. Keating, T. E. Mallouk, *Appl. Phys. Lett.* **2001**, *79*, 3392; d) L. E. Gutierrez-Rivera, L. Cescato, *J. Micromech. Microeng.* **2008**, *18*.
[11] J. Henzie, M. H. Lee, T. W. Odom, *Nat. Nanotechnol.* **2007**, *2*, 549.
[12] H. F. Ghaemi, T. Thio, D. E. Grupp, T. W. Ebbesen, H. J. Lezec, *Phys. Rev. B* **1998**, *58*, 6779.
[13] C. Genet, M. P. van Exter, J. P. Woerdman, *Opt. Commun.* **2003**, *225*, 331.
[14] A. Krishnan, T. Thio, T. J. Kima, H. J. Lezec, T. W. Ebbesen, P. A. Wolff, J. Pendry, L. Martin-Moreno, F. J. Garcia-Vidal, *Opt. Commun.* **2001**, *200*, 1.
[15] W. L. Barnes, *J. Opt. A—Pure Appl. Op.* **2006**, *8*, S87.
[16] Q. Xie, M. H. Hong, H. L. Tan, G. X. Chen, L. P. Shi, T. C. Chong, *J. Alloy Compd.* **2008**, *449*, 261.
[17] J. de Boor, D. S. Kim, V. Schmidt, *Opt. Lett.* **2010**, *35*, 3450.
[18] R. Murillo, H. A. van Wolferen, L. Abelmann, J. C. Lodder, *Microelectron. Eng.* **2005**, *78–79*, 260.
[19] T. C. Hennessy, *Lithography: Principles, Processes and Materials*, Noba Science Publishers, Inc., Hauppauge, NY, USA **2011**.